



# Purified myelin lipids display a critical mixing point at low surface pressure

Julio M. Pusterla<sup>a,b</sup>, Sergio A. Cannas<sup>c</sup>, Emanuel Schneck<sup>b</sup>, Rafael G. Oliveira<sup>a,\*</sup>

<sup>a</sup> Centro de Investigaciones en Química Biológica de Córdoba (CIQUIBIC)-Departamento de Química Biológica Ranwel Caputto, Facultad de Ciencias Químicas, Universidad Nacional de Córdoba, Haya de la Torre y Medina Allende, Ciudad Universitaria, X5000HUA Córdoba, Argentina

<sup>b</sup> Institut für Physik Kondensierter Materie, Technische Universität Darmstadt, Hochschulstrasse 8, 64289 Darmstadt, Germany

<sup>c</sup> Instituto de Física Enrique Gaviola (IFEG-CONICET), Facultad de Matemática Astronomía Física y Computación, Universidad Nacional de Córdoba, 5000 Córdoba, Argentina

## ARTICLE INFO

### Keywords:

Langmuir monolayers  
Myelin lipids  
Membrane domains  
Critical mixing point  
Line tension  
Dipolar repulsion

## ABSTRACT

Lipids extracted from Purified Myelin Membranes (LPMM) were spread as monomolecular films at the air/aqueous interface. The films were visualized by Brewster Angle Microscopy (BAM) at different lateral pressures ( $\pi$ ) and ionic environments. Coexistence of Liquid-Expanded (LE) and cholesterol-enriched (CE) rounded domains persisted up to  $\pi \approx 5$  mN/m but the monolayers became homogeneous at higher surface pressures. Before mixing, the domains distorted to non-rounded domains. We experimentally measured the line tension ( $\lambda$ ) for the lipid monolayers at the domain borders by a shape relaxation technique using non-homogeneous electric fields. Regardless of the subphase conditions, the obtained line tensions are of the order of pN and tended to decrease as lateral pressure increased toward the mixing point. From the mean square displacement of nested trapped domains, we also calculated the dipole density difference between phases ( $\mu$ ). A non-linear drop was detected in this parameter as the mixing point is approached. Here we quantitatively evaluated the  $\pi$ -dependance of both parameters with proper power laws in the vicinity of the critical mixing surface pressure, and the exponents showed to be consistent with a critical phenomenon in the two-dimensional Ising universality class. This idea of bidimensionality was found to be compatible only for simplified lipidic systems, while for whole myelin monolayers, that means including proteins, no critical mixing point was detected.

Finally, the line tension values were related with the thickness differences between phases ( $\Delta t$ ) near the critical point.

## 1. Introduction

Both pure lipids and mixture of lipids spontaneously self-assemble at fluid–fluid interfaces into two-dimensional (2D) monomolecular films [1]. These films often exhibit coexisting phases at the air–water interface which can be observed by optical techniques such as Fluorescence Microscopy (FM) or Brewster Angle Microscopy (BAM) [2–5].

Over the last years, the study of lateral heterogeneity in lipid membranes gained relevance due to its potential relation with signaling and trafficking phenomena taking place in cell membranes. The paradigm of lipid rafts theory intensified the study of liquid–liquid phase separation in complex lipidic biomembranes [6,7]. One of these assessments is concerned with the size and shape regulation of domains in planar

monolayers [8,9]. Other topic of particular interest is the phase coexistence characterization and eventual mixing–demixing transitions [10].

The morphology of lipid monolayers arises from a balance between long and short-range forces [11–15]. Amphiphilic molecules at the air–water interface have a resultant dipole moment, of which only the component perpendicular to interface plane is not cancelled in liquid layers [16,17]. This notion entails the existence of an electrostatic repulsive force between adjacent molecules even in the absence of charges, between domain–internal parts and between domains with higher dipole densities [18]. For coexisting liquid phases, the dipolar repulsion can be estimated through the difference in dipole density ( $\mu = \mu_{LE} - \mu_{CE}$ ) of the two phases. This dipole density difference is an electrostatic interaction resulting in a long-range force and its prevalence

**Abbreviations:** BAM, Brewster angle microscopy; LPMM, Lipids extracted from Purified Myelin Membranes; LE, Liquid-Expanded; CE, Cholesterol-enriched; 2D, two-dimensional; FM, Fluorescence Microscopy; IS, Ionic Strength.

\* Corresponding author.

**E-mail addresses:** [julio.pusterla@pkm.tu-darmstadt.de](mailto:julio.pusterla@pkm.tu-darmstadt.de) (J.M. Pusterla), [cannas@famaf.unc.edu.ar](mailto:cannas@famaf.unc.edu.ar) (S.A. Cannas), [emanuel.schneck@pkm.tu-darmstadt.de](mailto:emanuel.schneck@pkm.tu-darmstadt.de) (E. Schneck), [rafael.oliveira@unc.edu.ar](mailto:rafael.oliveira@unc.edu.ar) (R.G. Oliveira).

<https://doi.org/10.1016/j.bbamem.2022.183874>

Received 29 October 2021; Received in revised form 26 January 2022; Accepted 27 January 2022

Available online 2 February 2022

0005-2736/© 2022 Elsevier B.V. All rights reserved.

drives small non-circular domain shapes. It should be noted that not only the lipids but also the headgroup-hydrating water molecules contribute to the effective dipole density.

In contrast to electrostatic forces, line tension ( $\lambda$ ) is a short-range force that favors big circular domains. Line tension arises from the energy penalty associated with the phase boundaries. It is known that line tension not only influences the equilibrium shapes and coarsening kinetics of lipid domains but also modulates some biological processes [19–21] and drives certain membrane shape transitions [22].

It can therefore be inferred that domain patterns arise from a competition of forces in bidimensional systems. In particular, a line tension increase promotes large circular domains to the detriment of small and/or elongated domains.

According to McConnell [23], an equilibrium radius ( $R_{eq}$ ) arises from a competition between line tension and surface dipole densities differences, such that when  $R > e^{1/3} R_{eq}$  the domains lose circularity and adopt elongated shapes, where:

$$R_{eq} = \frac{e^3 \delta}{4} \exp \lambda / \mu^2 \quad (1)$$

$\delta$  is a nearest-neighbor intermolecular distance between the equivalent dipoles and  $e$  is the exponential, 2.718.

Our group has characterized Purified Myelin Membranes (PMM) over the last years and has shown that PMM monolayers exhibit a biphasic pattern along the whole  $\pi$  range almost up to the collapse. One of these phases, called Liquid-Expanded (LE phase), is enriched in high-molecular weight species with an expanded behavior, such as proteins and certain lipids, while another phase is mostly lipidic and enriched in cholesterol and cerebroside (CE phase) [24]. Additionally, it has been shown that the presence of salts stabilizes the phase separation not only in monolayers [2,25] but also in multilamellar arrangements [26,27]. Unlike whole PMM, when proteins are depleted from the system the purely lipidic monolayers (LPMM) homogenizes around 4–5 mN/m [3].

In this work, we studied the mixing behavior of the lipid fraction of myelin (LPMM).

We measured  $\lambda$  of LPMM monolayers using a method based on domain deformations induced by non-homogeneous electric fields [28]. We also measured the dipole density difference  $\mu$  of the two phases by observing the amplitude of Brownian motion of lipid domains in electrostatic traps [18]. From the analysis of both experimentally independent measurements the critical exponents for  $\lambda$  and  $\mu$ , termed  $\nu$  and  $\beta$ , respectively, were obtained using proper power law fits. We also assessed whether or not these exponents are characteristic of the universality class of the 2D Ising model phase transition. This theoretical model describes a critical phase transition in 2 or more dimensions and has been exactly solved in two dimensions for the case of nearest neighbor interactions between components [29]. The critical exponents of the transition are universal values and characterize the singular properties of physical quantities inside a universality class, which in this case are in the framework of the 2D Ising model [30–32].

The measurements were carried out at low ionic strength, physiological conditions, and in presence of calcium to set equivalent conditions with previous works performed by our group on purified whole myelin [25–27]. In this sense, it was already shown for PMM monolayers and multilayers that the presence of salts, especially of divalent calcium ions, increases the thickness difference between phases and stabilizes the phase separation [2,25,26].

## 2. Materials and methods

### 2.1. LPMM isolation and monolayer preparation

Highly purified myelin was extracted from bovine spinal cord by following a standard protocol [33]. For isolation of total myelin lipid extract, the lower solvent phase of a Folch's partition [34] of the

previously purified myelin was equilibrated (in proportion 1:1) with a chloroform–methanol–water (3:48:47) upper phase solution saturated with potassium citrate (0.1 M). Chloroform > 99%, Methanol 99.8% and Potassium citrate monobasic  $\geq 98.0\%$  were purchased from Merck KGaA (Germany), and used without further purification.

In this condition, the Folch's proteolipid becomes insoluble and can be removed because it accumulates at the two-solvent interface [35]. The procedure is repeated three times. Subsequently, the lower phase is washed with a citrate-free upper phase (in proportion 1:1). The myelin lipid extract is mainly composed by cholesterol (0.38), phosphatidylethanolamine (0.19), cerebroside (0.15), sphingomyelin (0.08), phosphatidylcholine (0.06), phosphatidylserine (0.05) and sulfatide (0.04) in mole fraction [36].

The lipids were spread directly at the air/aqueous interface from the resulting solution [3] and a Langmuir film balance (Microtrough, Kibron, Helsinki, Finland) was used to perform the experiments. Typical uncertainties in measurements via Wilhelmy plates of the surface pressure ( $\pi$ ) were  $\pm 1$  mN/m.

The solutions used as subphases were the following:

- Solution of low ionic strength (IS): Tris 5 mM, pH = 7.4
- Solution with near-physiological conditions: NaCl 150 mM in Tris 5 mM, pH = 7.4
- Solution with CaCl<sub>2</sub>: CaCl<sub>2</sub> 20 mM in Tris 5 mM, pH = 7.4

### 2.2. Fluorescence Microscopy (FM)

To distinguish monolayer phases using FM, the fluorescent probe 1- $\alpha$ -phosphatidylethanolamine - N - (lissamine rhodamine B sulfonyl) ammonium salt (chicken egg-transphosphatidylated), purchased from Avanti Polar Lipids Inc., was incorporated in the lipid solution before spreading in a molar fraction of 0.01. The fluorescent probe concentration in the cholesterol-enriched phase is lower, and thus this phase appears darker in the micrographs.

The Langmuir trough was placed on the stage of an inverted fluorescence microscope (Axiovert 200, Carl Zeiss, Oberkochen, Germany) with a 20 $\times$  objective and images were registered with a back-illuminated EMCCD video camera iXon 897 (Andor).

### 2.3. Experimental approach for the determination of dipole density differences ( $\mu$ )

To determine the difference of dipole density ( $\mu$ ) between two phases in a lipid monolayer a model proposed by McConnell's group was used [18]. According to this model the lipid molecules, associated water and eventually ions configure an in-plane two-dimensional array of dipoles. The number of dipoles is assumed to be equivalent to the number of molecules present at the air-water interface. Furthermore, it is considered for liquid phases that dipoles are oriented on average in a perpendicular direction to the monolayer plane, canceling by symmetry the horizontal components.

The difference of dipole densities between two phases  $\mu$  in isotropic bidimensional fluids is related to the normalized displacement from the center  $z$  of lipid domains in electrostatic traps. These traps are basically small circular domains of radii  $a$  electrostatically confined within larger circular domains of radii  $A$  (Fig. 1 and Movie S1 as Supplementary Material). The squared of  $\mu$  can be expressed as follows:

$$\mu^2 = \frac{2kT}{3\pi^2 \langle \bar{z} \rangle} \quad (2)$$

where  $k$  is the Boltzmann constant and  $T$  the absolute temperature. The parameter  $z$  accounts for the Brownian motion of a small lipidic domain inside an electrostatic trap [18]:

$$z = \frac{a^2 \rho^2}{A^3} \quad (3)$$

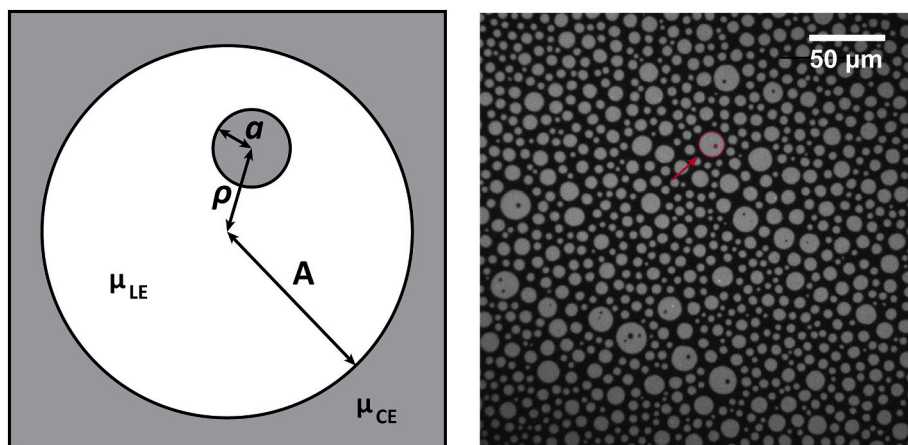


**Fig. 1.** Parameters used to calculate the dipole density differences. (Left) Here white and dark refer to domains that are strongly and weakly fluorescent. Three variables were measured for each domain system, namely, the radii of the inner and the outer domains ( $a$  and  $A$ ), and the displacement,  $\rho$ , of the inner domain from the center of the outer domain. (Right) Several nested electrostatic traps were chosen and analyzed for each condition over time and in at least 3 different monolayers. Red circle shows a typical example of a trap in a LPMM model monolayer. The white straight line represents a scale bar. (For interpretation of the references to colour in this figure legend, the reader is referred to the web version of this article.)

where  $a$ ,  $\rho$  and  $A$  are defined according to the following figure:

The software ImageJ 1.50 was used to measure  $a$ ,  $\rho$  and  $A$ . The  $z$  parameter is defined as the result of a single measurement,  $\langle z \rangle$  accounts for the mean value of a sequence of measurements over time for a given trap with radii  $a$  and  $A$ , and  $\langle \bar{z} \rangle$  refers to a whole average value among domains with the same or different radii  $a$  and  $A$  over several monolayers.

A total of 200–210 data points were measured from experiments on three different monolayers for each condition.

#### 2.4. Experimental approach for the determination of line tension ( $\lambda$ )

Line tension measurements were carried out according to Bischof et al. [28,37]. Briefly, LPMM monolayers at different lateral pressures were exposed to the action of an inhomogeneous electric field. For this purpose, one electrode was located roughly 200  $\mu\text{m}$  above the monolayer, while the other one was in contact with the subphase, and a potential difference of 300 V was applied. Since the electrostatic properties of domains and continuous phase are different, the field promotes a net force on the domains, and therefore they migrate to the region underneath the upper electrode. Domains get close together and “stripes” of the squeezed phase between domains develop. When domains coalesce, the stripes breakdown and the shape relaxes minimizing the length of domain boundaries. At this point, the electric field is turned off and the approximately constant retraction rate of the stripes is assessed. Stripe retraction is driven basically by two balanced forces: line tension force ( $F_\lambda$ ), which accelerates retraction, and friction force ( $F_\eta$ ), which slows it down. This leads to the expression:

$$\lambda = 4\eta_v g \frac{dL}{dt} \quad (4)$$

where  $\eta_v$  is the viscosity of the subphase, assumed as  $1 \times 10^{-3} \text{ Pa s}$ ,  $g$  is the average radius for the stripe head and  $\frac{dL}{dt}$  is the stripe retraction rate [28,37] (Movie S2 as Supplementary Material).

#### 2.5. Brewster angle microscopy

An EP3 single wavelength ellipsometer from Accurion (Göttingen) with an antivibration system (Vario 40–100) from the same manufacturer was used in BAM setup, i. e. light polarized in the plane ( $p$ ) of incidence, from a laser of 532 nm wavelength (50 mW) at the Brewster angle. A Langmuir Minitrough (KSV, Helsinki) via Wilhelmy plate was mounted on top of the ellipsometer stage.

Gray levels of each phase were measured by analyzing 10–20 micrographs acquired via CCD camera. For that, the gray level of a certain Region of Interest (ROI) of each phase was determined using the software ImageJ 1.50, and converted to reflected light intensity ( $R_p$ ) with suitable calibration, taking into account the calibration factor and the dark signal. This allows to measure  $R_p$  even in heterogeneous monolayers at specific domains.

For the evaluation of the refractive indexes ( $n$ ) of the film we used a method developed by our group [38] and previously tested with myelin lipid fraction [38], whole purified myelin [25] and sterol films [39], based on the best contrast matching by controlling the subphase refractive index ( $n_2$ ).

#### 2.6. Monolayer thickness determination

By knowing the refractive index and  $R_p$  of both phases at all surface pressures, we calculated the film thickness ( $t$ ). For this, the gray level of each section of the micrographs was converted to  $R_p$ , and the thickness was calculated assuming a film of refractive index  $n$  and with  $t$  much

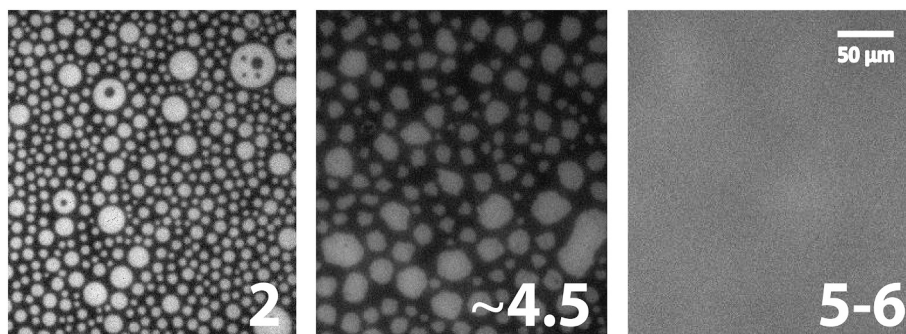


**Fig. 2.** FM micrographs of LPMM monolayers at low IS. The sequence was taken at different  $\pi$  values (white numbers, in mN/m). The white straight line represents a scale bar.

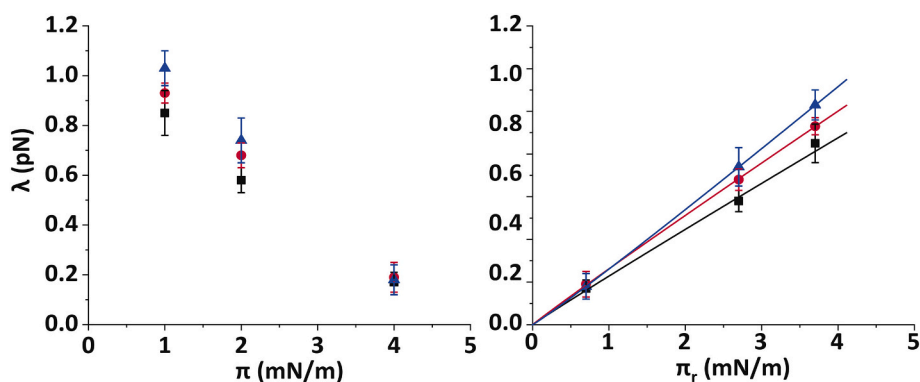


**Fig. 3.** (Left)  $\lambda$  vs  $\pi$  for LPMM monolayers in low IS (black dots), physiological condition (red dots) and with  $\text{CaCl}_2$  (blue dots) subphases. The error bars correspond to the standard deviation of 4 independent determinations of  $\lambda$  for each condition. (Right) The data from the graph on the left were plotted against reduced surface pressure  $\pi_r = \pi_c - \pi$ , and fitted according to Eq. (6) to obtain the values of critical exponent  $\nu$ .  $\pi_c$  was held fixed in 4.7 mN/m. (For interpretation of the references to colour in this figure legend, the reader is referred to the web version of this article.)

smaller than the incident light wavelength ( $\lambda$ ) [40,41], giving:

$$t = \frac{\sqrt{R_p}}{\sin(2\theta_B - 90)} \left( \frac{\pi \sqrt{n_1^2 + n_2^2} (n_1^2 - n^2) (n_2^2 - n^2)}{\Lambda (n_1^2 - n_2^2) n^2} \right) \quad (5)$$

Here  $n_1$  is the refractive index of air (assumed as 1), and  $\pi$  is the irrational number.

### 3. Results and discussion

#### 3.1. Morphology of LPMM monolayers

The compression isotherms of LPMM monolayers are consistent with the ones previously published [42] and there is also no significant influence of the subphase type on the surface behavior. As previously reported, the LPMM monolayers exhibit two coexisting phases at very low surface pressures ( $\pi \leq 5$  mN/m) but around 5 mN/m the domains boundaries turn irregular and the monolayer becomes homogeneous (Fig. 2) [3,43].

For this system, no substantial differences in the morphological pattern are observed by presence of salts (Tris, physiological condition and presence of calcium) in the subphase. Our experimental critical pressure ( $\pi_c$ ) was always found to be between 4.5 and 5 mN/m for all the subphase types. Unlike the LPMM monolayers, our group has already reported that for whole PMM monolayers (with proteins included) the presence of salts promotes the lateral phase separation over the entire range of  $\pi$  while only at low IS the monolayer homogenizes at 37–38 mN/m [2,25].

#### 3.2. Line tension analysis in LPMM monolayers

As mentioned before, high line tensions ( $\lambda$ ) tend to correlate with strongly different properties of the two coexisting phases.

Fig. 3 (left) shows the  $\lambda$  variation in the narrow range of  $\pi$  where phase coexistence is observed. From 0 to 5 mN/m the line tension decreases from  $\lambda > 1$  pN down to  $\lambda < 0.2$  pN when approaching  $\pi_c$ . Indeed, low line tensions ( $< 1$  pN) have been previously reported near critical points for other systems [44–46].

The values fall into the typical range experimentally found for lipid systems [47,48]; but they do not match the values calculated in the past for lipids mimicking myelin systems, for which  $\lambda$  values as low as 3.5–11.3 fN were reported [49]. However, those estimates were based on the assumption of equilibrium domain size distributions, which may not necessarily be fulfilled in multicomponent systems. In fact, as discussed by Bischof et al. [37], observations of equilibrium configurations are very unlikely because they usually are not accomplished on experimentally accessible time scales [50,51]. Furthermore, there are indications that  $\lambda$  values below 0.3 pN would not be effective in maintaining stable domains [52].

Regarding the ionic environment, the presence of calcium increases  $\lambda$

**Table 1**

Measured critical exponents  $\nu$  and  $\beta$  for all three subphase types.

	$\lambda = m[\pi_r]^\nu$	$\mu^2 = s[\pi_r]^{2\beta}$
	Exponent $\nu$	Exponent $\beta$
Low IS	$0.97 \pm 0.12$	$0.18 \pm 0.04$
Physiological condition	$0.98 \pm 0.04$	$0.11 \pm 0.02$
With calcium	$1.02 \pm 0.01$	$0.09 \pm 0.04$

values slightly but the effect is not as pronounced as in PMM monolayers [25], indicating a crucial role of the myelin proteins in the magnitude of  $\lambda$  and therefore in the phase separation stability.

The behavior of LPMM monolayers could be explained due to the proximity to a critical point, considering line tension as a measure of the stability of phase coexistence. The critical surface pressure for mixing is defined as the pressure when the monolayer homogenizes over the apex of the phase diagram (spinodal decomposition). Not only the line tension values drop and the domains become rough, but also the critical surface pressure for mixing is related with line tension according to [30,47]:

$$\lambda = m[\pi_r]^\nu \quad (6)$$

where  $m$  and  $\nu$  are adjustable parameters and  $\pi_r$  is the reduced surface pressure, defined as  $\pi_r = \pi_c - \pi$ .

The data in Fig. 3 (right panel) were fitted according to Eq. (6) considering that  $\pi_c = 4.7$  mN/m for all the ionic conditions. The calculated  $\nu$  values are summarized in Table 1 (1st column), and they are close to  $\nu \approx 1$  as expected in accordance with the Ising model for a 2-D system [30–32].

It has been previously shown that line tension decreases and becomes zero at the critical point and linear relations between  $\lambda$  and  $\pi$  ( $\lambda = m[\pi_r]^\nu$ , with  $\nu \approx 1$ ) [47,48], and also between  $\lambda$  and  $T$  ( $\lambda = m[T_r]^\nu$ , with  $\nu \approx 1$ ) [53] have been reported.

Here, we determined the critical exponent for the  $\pi$ -dependence of the line tension near the critical point in a complex biomembrane (LPMM) using a different experimental technique and the measured values are consistent with a critical phenomenon in the two-dimensional Ising universality class.

#### 3.3. Dipole density differences analysis in LPMM monolayers

The dipole density difference between phases  $\mu$  was experimentally determined through the Brownian motion analysis of small domains of one phase electrostatically trapped in the center of a larger spherical domain of the other phase, as schematically depicted in Fig. 1. The employed model [18] relates  $\mu^2$  with the mean squared displacement of the small domains from the center of the hosting domains. The instantaneous displacement  $z$  (see Eq. (3)) was recorded at each ionic condition and histograms were built (Fig. 4, left). The theoretical probability

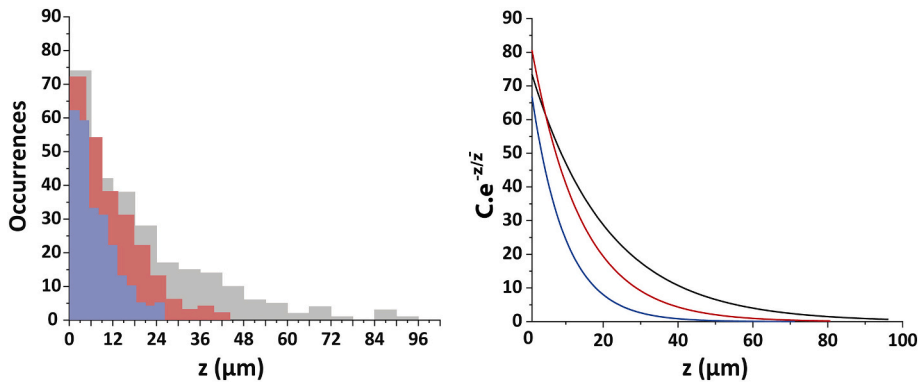


**Fig. 4.** (Left) Example of occurrence-frequency histograms for the variable  $z$  on the different subphase conditions: low IS (gray/black), physiological condition (red) and presence of calcium (blue) at 2 mN/m. (Right) Theoretical curves of  $P$  function are comparatively displayed superimposed for the three conditions. For the low IS subphase, in a total of 205 measurements,  $\bar{z} = 17.5 \mu\text{m}$  and  $C = 74.2$ ; for the physiological condition subphase, in a total of 206 measurements,  $\bar{z} = 12.6 \mu\text{m}$  and  $C = 75.6$  and for the subphase with calcium, in a total of 202 measurements,  $\bar{z} = 7.9 \mu\text{m}$  and  $C = 68.4$ . (For interpretation of the references to colour in this figure legend, the reader is referred to the web version of this article.)

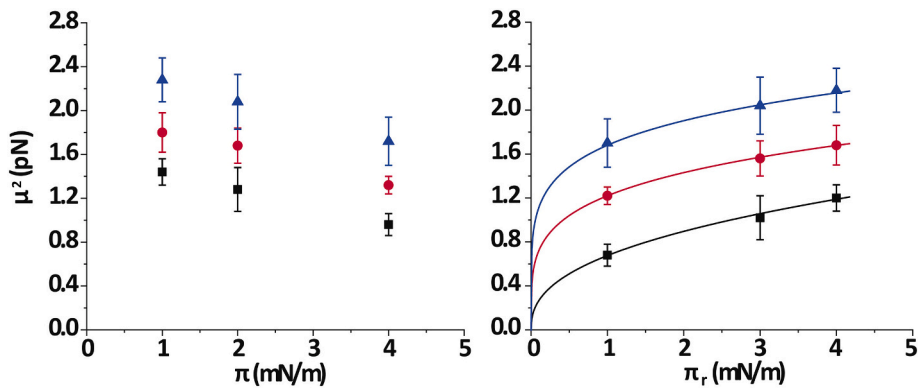


**Fig. 5.** (Left)  $\mu^2$  vs  $\pi$  for LPMM monolayers on low IS (black dots), physiological condition (red dots) and with  $\text{CaCl}_2$  (blue dots) subphases. The error bars correspond to the standard deviation of 6 independent determinations of  $|\mu|$  for each condition. (Right) The data from the graph on the left were plotted against  $\pi_r = \pi_c - \pi$  and fitted according to Eq. (7) to obtain the values of critical exponent  $\beta$ .  $\pi_c$  was held fixed in 4.7 mN/m as a good approximation of the experimental critical pressure. (For interpretation of the references to colour in this figure legend, the reader is referred to the web version of this article.)

distributions corresponding to the best-matching model parameters are shown in Fig. 4 (right).

$$P\left(\frac{z}{\bar{z}}\right) = C.e^{-\left(\frac{z}{\bar{z}}\right)} \quad (7)$$

Here,  $C$  is a normalization factor chosen so that the integral of  $P$  from 0 to infinity equals the area under the histogram.

Fig. 5 (left) shows  $\mu^2$  as a function of  $\pi$  up to 4 mN/m for LPMM monolayers. The orders of magnitude are the same as those  $\mu^2$  values reported previously by Benvegnu et al. using this method [54] or those ones measured from lipid monolayer domain boundary fluctuations [48]. Much like the line tension,  $\mu^2$  tends to decrease as surface pressure increases. Subphases with calcium promote higher  $|\mu|$ , i.e., stronger dipolar repulsion than physiological conditions. The lowest  $|\mu|$  is obtained for low-IS subphases. This result implies that the ionic strength of the subphase does not effectively screen the dipolar repulsion. On the contrary, the inclusion of ions could possibly enhance the dipolar density difference through differential binding as previously shown in purified myelin membranes [27] and headgroup-ordered monolayers of uncharged glycolipids [55].

As the line tension behavior, also  $\mu^2$  can be fitted near the critical point according to a scaling law, with the equation

$$\mu^2 = s[\pi_r]^{2\beta} \quad (8)$$

where  $s$  and  $\beta$  are adjustable parameters and the reduced surface pressure  $\pi_r = \pi_c - \pi$ .

There has been a wide range of estimates for the critical exponent  $\beta$ . Ising two-dimensional model predicts a value of  $\beta = 1/8$  (0.125) [56], a result also experimentally corroborated in monolayers of phospholipids [57], Ising-like crystals [58] and facet reconstruction of Au surface [59]. On the other hand, there is less evidence from experiments on lipid

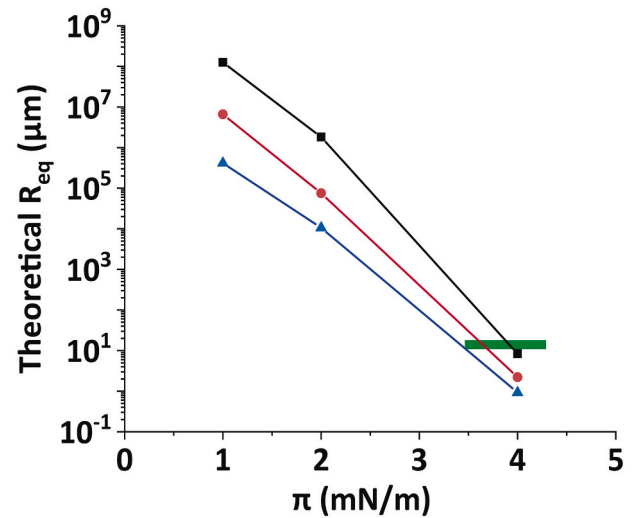


**Fig. 6.** Calculated  $R_{eq}$  vs  $\pi$  for LPMM monolayers in low IS (black dots), physiological condition (red dots) and with  $\text{CaCl}_2$  (blue dots) subphases. As can be seen, only on the vicinity of the critical mixing point the values are close to the equilibrium radii. The green line shows a  $\pi$ -range ( $\sim 3.5$  to  $4.2$  mN/m) where the experimental  $R_{eq}$  falls from  $\sim 10$  to  $14 \mu\text{m}$ , without significant differences between each ionic condition. (For interpretation of the references to colour in this figure legend, the reader is referred to the web version of this article.)

monolayers [48] that  $\beta$  could be closer to  $1/3$ , which is the prediction of Ising model for a three-dimensional system [56].

Here, the data were fitted (Fig. 5-right) according to Eq. (7) considering again that  $\pi_c = 4.7$  mN/m for all ionic conditions. The

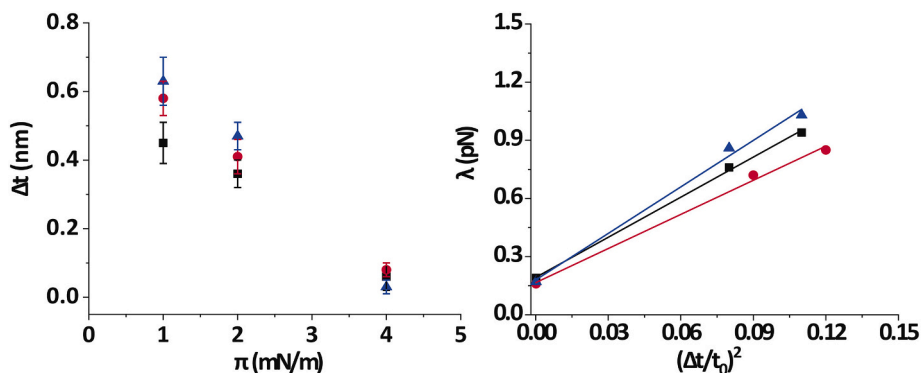


Fig. 7. (Left)  $\Delta t$  vs  $\pi$  for LPMM on subphases of low IS (black dots), physiological condition (red dots) and with calcium (blue dots). (Right)  $\lambda$  vs  $(\Delta t/t_0)^2$  between phases. (For interpretation of the references to colour in this figure legend, the reader is referred to the web version of this article.)

obtained  $\beta$  values are summarized in Table 1 (2nd column). The values cluster near the prediction of 2D Ising model  $\beta = 1/8$ , but far away from the predictions of the 3D Ising model ( $\beta = 1/3$ ) as well as the one of mean field theory ( $\beta = 1/2$ ).

### 3.4. Theoretical equilibrium radius

As mentioned above, the model proposed by McConnell allows to calculate a theoretical equilibrium radius  $R_{eq}$  (Eq. (1)) based on the relation  $\lambda/\mu^2$ . This model and the ones related has been tested in simple lipid mixtures [47], but also in complex ones as model myelin lipid monolayers [49].

We show here that departure from the critical condition leads to exceedingly large calculated values for  $R_{eq}$  (Fig. 6). Only when approaching to the mixing point the calculated equilibrium radii (0–20  $\mu\text{m}$ ) fall into the range of the experimental observations. Although not explained, this discrepancy was early noticed [47], but this fact is usually neglected. This huge discrepancy precludes of applying this theoretical model far away from the critical point. This in turn could explain the very low  $\lambda$  values calculated from distribution of lipid mixtures mimicking myelin domains based on the theory of McConnell [49]. A further complication could be related to the equilibrium condition for the domain size distribution. Satisfying such an equilibrium condition can be beyond experimental time scales due to the slow kinetics of equilibration rates in monolayers size domains, in the order of days or weeks [50,51]. In this view, a perturbation strategy for the determination of  $\lambda$ , as was taken here, may be preferable. Alternatively, careful validation and/or calibration with proper standards should be mandatory before applying equilibrium-based techniques for line tension determination. Very close the critical point, nevertheless, high fluctuations in size and shapes could arise, hindering again applicability.

We checked experimentally that beyond radii of about 15–20  $\mu\text{m}$ , the circular domains become increasingly unstable and acquire more elliptical shapes; further increments of size lead to very elongated domains. According to McConnell [47] the domain distortion radii are bigger by a factor of  $e^{1/3}$  relative to  $R_{eq}$ . This would lead to experimental  $R_{eq}$  of 10–14  $\mu\text{m}$ , comparable to those theoretically calculated through the model in the vicinity of the critical point (Fig. 6).

### 3.5. Thickness differences and line tension

Line tension is known to depend on the hydrophobic mismatch between phases and on the ability of the molecules to deform and adapt to a different layer thickness [49,60–62]. In order to further explore the supramolecular basis of the mixing behavior we determined the thickness  $t$  (Eq. (5)) of each phase (LE and cholesterol-enriched) using BAM reflectivities ( $R_p$ ) and considering proper refractive indexes for each phase ( $n$ ) measured with a technique recently developed by our group

[38]. From such thickness values the thickness differences ( $\Delta t$ ) between domains and surrounding media can be determined. Fig. 7 (left) includes measurements from LPMM monolayers in subphases of low IS, physiological conditions, and in presence of calcium. As can be seen, the presence of salts mildly increases the thickness of the LE phase, and therefore the thickness mismatch. In this case, a relevant difference is also observed regarding PMM monolayers, for which the trend is similar but the thickness of the protein-enriched LE phase is much sensitive to changes in the ionic environment [25]. This effect translates as an increase in  $\Delta t$  when salts are present.

To inquire about the determinants to reach such low  $\lambda$  values in the vicinity of the critical point, we tested the model proposed by Cohen and Kuzmin [60]. Equations that relate  $\lambda$  with  $\Delta t$  have been theoretically derived by the Cohen's group [60,61] and used afterwards in order to derive  $\lambda$  from  $\Delta t$  [46]. According to this model, the line tension  $\lambda$  and the hydrophobic mismatch  $\Delta t$  are related as:

$$\lambda = A \frac{\Delta t^2}{t_0^2} - B \quad (9)$$

where  $t_0$  is the mean value of the height of the two phases:  $t_0 = (t_{LE} + t_{CE})/2$ ,  $t$  is the monolayer thickness; and  $A$  and  $B$  are positive parameters which depend on the elastic splay modulus, the tilt modulus and the spontaneous curvature of the monolayer.

Line tensions  $\lambda$  were plotted vs.  $\Delta t^2/t_0^2$  for  $\pi \leq 4$  mN/m and a remarkably linear correlation was observed, in line with Eq. (9) (Fig. 7-right). The positive intercept ( $B$  in Eq. (9)), indicative of the residual value for  $\lambda$  in the absence of thickness mismatch, may give account of lateral intermolecular interactions, such as hydrogen bonding, electrostatics or van der Waals interactions, which are not considered in this model.

In summary,  $\Delta t$  appears to be a key determinant for  $\lambda$ , but, as pointed out before, other parameters related to membrane deformation were found to contribute to  $\lambda$ , too, such as the membrane curvature [37,63].

### 3.6. Universality class

In analogy to what happens in liquid-liquid mixtures, where the order parameter is the difference in composition between the phases [30], our data support the idea that on approaching the critical mixing point the partition coefficient between both phases of the individual components tends to unity, which means the components redistribute more and more evenly between the two phases. This view is compatible with the observation that the thickness difference between the phases decreases, as well as also the line tension and the dipole density difference. The scaling exponents by which the two latter variables vanish support the idea that behavior of these monolayers indeed follows the universality class of the 2D Ising model. The dipole density difference in this case would qualify as order parameter, as it should be roughly

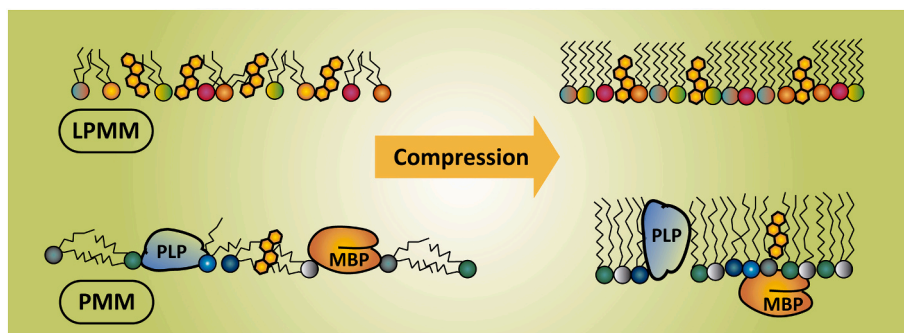


**Fig. 8.** Unlike the lipid fraction, in the whole myelin monolayers the MBP is squeezed out over 20 mN/m along the compression and the system eventually loses its 2D-dimensionality.

proportional to the difference in the chemical composition. The predicted value for the critical exponent  $\beta$  according to the 2D Ising model is  $1/8$  [31,32], and this value agrees very well with the critical exponent determined in this work, which differs from the exponents for 3D Ising model ( $1/3$ ) and the mean field theory ( $1/2$ ). The critical exponent  $\nu$  of  $\lambda$  also fits in the 2D Ising model prediction (1.0) in contrast to the predicted 3D Ising model ( $\sim 0.63$ ) or the mean field theory ( $1/2$ ) [30–32]. Comparable measurements to those reported in this work have been previously obtained for Langmuir monolayers using different experimental techniques [57].

### 3.7. Lipid raft hypothesis

The Ising model would make place for the hypothesis of lipid rafts, because nanometric domains could exist in hypercritical conditions, beyond the critical point. Nevertheless, we have determined that the equilibrium condition between myelin lipid monolayers and its corresponding bilayers is around 46 mN/m at the closest lateral packing just before collapse [64,65], that is far beyond the critical mixing point which is as low as 4.7 mN/m. As nanometric domains completely homogenizes far away from the critical point, then it could be that the monolayer is completely homogeneous at the bilayer molecular packing.

### 3.8. Comparison between whole myelin membranes (PMM) and their lipid fraction (LPMM)

Unlike LPMM monolayers, for whole PMM monolayers (with proteins included) no critical mixing points were identified [25]. The homogenization in PMM monolayers is only reached at high  $\pi$  (37–40 mN/m) and at low IS. Moreover, the measured  $\lambda$  values could not be fitted with Eq. (6) to determine  $\pi_c$ , which discards a critical phenomenon. Taking into account that whole myelin multilayers have a mixing point between room and physiological temperature [26,66], we hypothesize that the presence of proteins could alter the phase behavior of myelin due to the perturbation of these transmembrane proteins, whose conformation can be artifactual in monomolecular films [2]. Moreover, it was previously shown that Myelin Basic Protein is squeezed out at around 20 mN/m remaining peripherally associated to the lipid monolayer, in this case a 2D system cannot apply any longer [43,67]. This problem of the monolayer model system does not apply to the LPMM, which is a simpler 2D system with molecules side by side (Fig. 8). Certainly, in order to capture the essential features of the myelin membrane (i. e. universality class) by using Langmuir monolayers, a simplified system (whole lipid extract) might in fact be more suitable than the whole natural system (protein included) due to the unnatural state of transmembrane proteins in monolayers at the air/water interface.

## 4. Conclusion

In this work we showed that the lipid fraction of Purified Myelin Membranes (LPMM) displays a critical mixing point at low lateral pressure ( $\sim 5$  mN/m). The line tension and the difference in the dipole density between phases were measured independently in LPMM monolayers by setting up experimental methods based on a shape relaxation technique using inhomogeneous electric fields and the Brownian motion of lipid domains in electrostatic traps, respectively. Both parameters were found to decrease with a power law dependence as the surface pressure approached the phase transition pressure ( $\pi_c$ ), and the exponents values  $\nu$  and  $\beta$  showed to be in agreement with a critical phenomenon in the two-dimensional Ising universality class.

By comparing the behavior of LPMM monolayers with the whole myelin monomolecular films, the latter not showing a critical mixing point at low lateral pressures, we conclude that the presence of proteins plays a key role in phase state of myelin by altering the 2D behavior of the simpler lipidic mixture.

Finally, the presence of calcium in LPMM monolayers has an effect in the same direction but weaker than for whole PMM. The line tension and thickness differences are higher for the system with calcium, correlating with the phase coexistence stabilization that such ion promotes in the phase diagram of myelin [27].

Supplementary data to this article can be found online at <https://doi.org/10.1016/j.bbmem.2022.183874>.

### CRediT authorship contribution statement

**Julio Pusterla:** Conceptualization, Data Curation, Formal analysis, Investigation, Methodology, Writing-original draft and review & editing.

**Sergio Cannas:** Writing-review & editing.

**Emanuel Schneck:** Writing-review & editing.

**Rafael Oliveira:** Conceptualization, Investigation, Methodology, Writing-original draft and review & editing, Supervision, Funding Acquisition and Project Administration.

### Declaration of competing interest

The authors declare that they have no known competing financial interests or personal relationships that could have appeared to influence the work reported in this paper.

### Acknowledgements

Prof. RGO is a carrier researcher at the *National Scientific and Technical Research Council* (CONICET, Argentina). JP is a former PhD fellow from CONICET. We wish to thank to CEMINCO and the National Microscopy System (SNM, MinCyT, Argentina) for access to Brewster Angle and Fluorescence Microscopy. This work was supported by grants from

CONICET, MINCYT, SECyT (UNC) from Argentina and Alexander von Humboldt Foundation from Germany. JP and ES gratefully acknowledge financial support by the German Research Foundation (DFG) via an Emmy-Noether grant (SCHN 1396/1).

## References

- [1] J.N. Israelachvili, Intermolecular and surface forces, 3rd ed., Academic Press, 2011.
- [2] R.G. Oliveira, E. Schneck, S.S. Funari, M. Tanaka, B. Maggio, Equivalent aqueous phase modulation of domain segregation in myelin monolayers and bilayer vesicles, *Biophys. J.* 99 (2010) 1500–1509.
- [3] C.M. Rosetti, R.G. Oliveira, B. Maggio, The folch-lees proteolipid induces phase coexistence and transverse reorganization of lateral domains in myelin monolayers, *Biochim. Biophys. Acta, Biomembr.* 1668 (2005) 75–86.
- [4] R.G. Oliveira, B. Maggio, Epifluorescence microscopy of surface domain microheterogeneity in myelin monolayers at the air-water interface, *Neurochem. Res.* 25 (2000) 77–86.
- [5] S. Hénon, J. Meunier, Microscope at the Brewster angle: direct observation of first-order phase transitions in monolayers, *Rev. Sci. Instrum.* 62 (1991).
- [6] K. Simons, E. Ikonen, Functional rafts in cell membranes, *Nature* 387 (1997) 569–572.
- [7] M. Edidin, The state of lipid rafts: from model membranes to cells, *Annu. Rev. Biophys. Biomol. Struct.* 32 (2003) 257–283.
- [8] H.M. McConnell, Theory of hexagonal and stripe phases in monolayers, *Proc. Natl. Acad. Sci. U. S. A.* 86 (1989) 3452–3455.
- [9] S. Wurlitzer, T.M. Fischer, H. Schmiedel, Equilibrium size of circular domains in langmuir monolayers, *J. Chem. Phys.* 116 (2002).
- [10] S.L. Keller, W.H. Pitcher III, W.H. Huestis, H.M. McConnell, Red blood cell lipids form immiscible liquids, *Phys. Rev. Lett.* 81 (1998).
- [11] H.M. McConnell, Structures and transitions in lipid monolayers at the air-water interface, *Annu. Rev. Phys. Chem.* 42 (1991) 171–195.
- [12] V.M. Kaganer, H. Möhwald, P. Dutta, Structure and phase transitions in Langmuir monolayers, *Rev. Mod. Phys.* 71 (1999) 779–819.
- [13] J.M. Barakat, T.M. Squires, Shape morphology of dipolar domains in planar and spherical monolayers, *J. Chem. Phys.* 152 (2020), 234701.
- [14] R.E. Goldstein, D.P. Jackson, Domain shape relaxation and the Spectrum of thermal fluctuations in Langmuir monolayers, *J. Phys. Chem.* 98 (1994) 9626–9636.
- [15] M. Seul, D. Andelman, Domain shapes and patterns: the phenomenology of modulated phases, *Science* 267 (1995) 476–483.
- [16] J.M. Smaby, H.L. Brockman, Surface dipole moments of lipids at the argon-water interface. Similarities among glycerol-ester-based lipids, *Biophysical Journal* 58 (1990) 195–204.
- [17] H. Brockman, Dipole potential of lipid membranes, *Chem. Phys. Lipids* 73 (1994) 57–79.
- [18] H.M. McConnell, P.A. Rice, D. Benvegnu, Brownian motion of lipid domains in electrostatic traps in monolayers, *J. Phys. Chem.* 94 (1990) 8965–8968.
- [19] T. Baumgart, S.T. Hess, W.W. Webb, Imaging coexisting fluid domains in biomembrane models coupling curvature and line tension, *Nature* 425 (2003) 821–824.
- [20] T. Baumgart, S. Das, W.W. Webb, J.T. Jenkins, Membrane elasticity in giant vesicles with fluid phase coexistence, *Biophys. J.* 89 (2005) 1067–1080.
- [21] A. Tian, C. Johnson, W. Wang, T. Baumgart, Line tension at fluid membrane domain boundaries measured by micropipette aspiration, *Phys. Rev. Lett.* 98 (2007), 208102.
- [22] J. Liu, M. Kaksonen, D.G. Drubin, G. Oster, Endocytic vesicle scission by lipid phase boundary forces, *Proc. Natl. Acad. Sci. U. S. A.* 103 (2006) 10277–10282.
- [23] H.M. McConnell, V.T. Moy, Shapes of finite two-dimensional lipid domains, *J. Phys. Chem.* 92 (1988) 4520–4525.
- [24] R.G. Oliveira, B. Maggio, Compositional domain immiscibility in whole myelin monolayers at the air-water interface and Langmuir-Blodgett films, *Biochim. Biophys. Acta, Biomembr.* 1561 (2002) 238–250.
- [25] J. Pusterla, J.M. Hernandez, N. Wilke, E. Schneck, R.G. Oliveira, Ionic environment, thickness and line tension as determinants of phase separation in whole purified myelin membranes monolayers, *Colloids Surf. B Biointerfaces* 207 (2021), 112027.
- [26] J.M. Pusterla, E. Schneck, S.S. Funari, B. Deme, M. Tanaka, R.G. Oliveira, Cooling induces phase separation in membranes derived from isolated CNS myelin, *PLoS One* 12 (2017), e0184881.
- [27] J.M. Pusterla, E. Schneck, R.G. Oliveira, Phase diagram of purified CNS myelin reveals continuous transformation between expanded and compacted lamellar states, *Cells* 9 (2020).
- [28] A.A. Bischof, N. Wilke, Molecular determinants for the line tension of coexisting liquid phases in monolayers, *Chem. Phys. Lipids* 165 (2012) 737–744.
- [29] L. Onsager, Crystal statistics. I. A two-dimensional model with an order-disorder transition, *Phys. Rev.* 65 (1944).
- [30] A.R. Honerkamp-Smith, S.L. Veatch, S.L. Keller, An introduction to critical points for biophysicists; observations of compositional heterogeneity in lipid membranes, *Biochim. Biophys. Acta, Biomembr.* 1788 (2009) 53–63.
- [31] N. Goldenfeld, Lectures on Phase Transitions and the Renormalization, Group Addison-Wesley, New York, 1992.
- [32] J.S. Rowlinson, B. Widom, Molecular Theory of Capillarity, Dover Publications Inc, 2002.
- [33] J.E. Haley, F.G. Samuels, R.W. Ledeen, Study of myelin purity in relation to axonal contaminants, *Cell. Mol. Neurobiol.* 1 (1981) 175–187.
- [34] J. Folch, I. Ascoli, M. Lees, J.A. Meath, B.N. Le, Preparation of lipide extracts from brain tissue, *J. Biol. Chem.* 191 (1951) 833–841.
- [35] M.B. Lees, J.D. Sakura, Preparation of proteolipids, *Res. Meth. Neurochem.* (1978) 345–370.
- [36] R.G. Oliveira, R.O. Calderon, B. Maggio, Surface behavior of myelin monolayers, *Biochim. Biophys. Acta Biomembr.* 1370 (1998) 127–137.
- [37] A.A. Bischof, A. Mangiarotti, N. Wilke, Searching for line active molecules on biphasic lipid monolayers, *Soft Matter* 11 (2015) 2147–2156.
- [38] J.M. Pusterla, A.A. Malfatti-Gasperini, X.E. Puentes-Martinez, L.P. Cavalcanti, R. G. Oliveira, Refractive index and thickness determination in Langmuir monolayers of myelin lipids, *Biochim. Biophys. Acta Biomembr.* 2017 (1859) 924–930.
- [39] A. Mangiarotti, V.V. Galassi, E.N. Puentes, R.G. Oliveira, M.G. Del Popolo, N. Wilke, Hopanoids like sterols form compact but fluid films, *Langmuir* 35 (2019) 9848–9857.
- [40] C. Lheveder, S. Hénon, J. Meunier, Brewster angle microscopy, in: A. Baszkin, W. Norde (Eds.), *Physical Chemistry of Biological Interfaces*, Marcel Dekker Inc, New York, 2000, pp. 559–576.
- [41] N. Wilke, Lipid monolayers at the air-water interface: a tool for understanding electrostatic interactions and rheology in biomembranes, in: A. Iglič, C.V. Kulkarni (Eds.), *Advances in Planar Lipid Bilayers and Liposomes*, vol. 20, Academic Press, 2014, pp. 51–81.
- [42] C.M. Rosetti, B. Maggio, Protein-induced surface structuring in myelin membrane monolayers, *Biophys. J.* 93 (2007) 4254–4267.
- [43] C.M. Rosetti, B. Maggio, R.G. Oliveira, The self-organization of lipids and proteins of myelin at the membrane interface. Molecular factors underlying the microheterogeneity of domain segregation 1778 (2008) 1665–1675.
- [44] C. Esposito, A. Tian, S. Melamed, C. Johnson, S.Y. Tee, T. Baumgart, Flicker spectroscopy of thermal lipid bilayer domain boundary fluctuations, *Biophys. J.* 93 (2007) 3169–3181.
- [45] B.L. Stottrup, A.M. Heussler, T.A. Bibelnicks, Determination of line tension in lipid monolayers by Fourier analysis of capillary waves, *J. Phys. Chem. B* 111 (2007) 11091–11094.
- [46] A.J. Garcia-Saez, S. Chiantia, P. Schuille, Effect of line tension on the lateral organization of lipid membranes, *J. Biol. Chem.* 282 (2007) 33537–33544.
- [47] D. Benvegnu, H.M. McConnell, Line tension between liquid domains in lipid monolayers, *J. Phys. Chem.* 96 (1992) 6820–6824.
- [48] M.C. Heinrich, I. Levental, H. Gelman, P.A. Janmey, T. Baumgart, Critical exponents for line tension and dipole density difference from lipid monolayer domain boundary fluctuations, *J. Phys. Chem. B* 112 (2008) 8063–8068.
- [49] D.W. Lee, Y. Min, P. Dhar, A. Ramachandran, J.N. Israelachvili, J.A. Zasadzinski, Relating domain size distribution to line tension and molecular dipole density in model cytoplasmic myelin lipid monolayers, *Proc. Natl. Acad. Sci. U. S. A.* 108 (2011) 9425–9430.
- [50] H.M. McConnell, Equilibration rates in lipid monolayers, *Proc. Natl. Acad. Sci. U. S. A.* 93 (1996) 15001–15003.
- [51] K.B. Towles, N. Dan, Line tension and coalescence in heterogeneous membranes, *Langmuir* 23 (2007) 13053–13058.
- [52] R.D. Usery, T.A. Enoki, S.P. Wickramasinghe, M.D. Weiner, W.C. Tsai, M.B. Kim, S. Wang, T.L. Torng, D.G. Ackerman, F.A. Heberle, J. Katsaras, G.W. Feigenson, Line tension controls liquid-disordered + liquid-ordered domain size transition in lipid bilayers, *Biophys. J.* 112 (2017) 1431–1443.
- [53] A.R. Honerkamp-Smith, P. Cicuta, M.D. Collins, S.L. Veatch, M. den Nijs, M. Schick, S.L. Keller, Line tensions, correlation lengths, and critical exponents in lipid membranes near critical points, *Biophys. J.* 95 (2008) 236–246.
- [54] D. Benvegnu, H.M. McConnell, Surface dipole densities in lipid monolayers, *J. Phys. Chem.* 97 (1993) 6686–6691.
- [55] C. Stefanii, V.M. Latza, O. Gutowski, P. Fontaine, G. Brezesinski, E. Schneck, Headgroup-ordered monolayers of uncharged glycolipids exhibit selective interactions with ions, *J. Phys. Chem. Lett.* 10 (2019) 1684–1690.
- [56] J.S. Rowlinson, B. Widom, Interfaces near critical points, in: *The Molecular Theory of Capillarity*, Clarendon Press, Oxford, 1982.
- [57] J.P. Hagen, H.M. McConnell, Liquid-liquid immiscibility in lipid monolayers, *Biochim. Biophys. Acta, Biomembr.* 1329 (1997) 7–11.
- [58] E.J. Samuelsen, Critical behaviour of the two-dimensional Ising antiferromagnets K<sub>2</sub>CoF<sub>4</sub> and Rb<sub>2</sub>CoF<sub>4</sub>, *J. Phys. Chem. Solids* 35 (1974) 785–793.
- [59] J.C. Campuzano, M.S. Foster, G. Jennings, R.F. Willis, W. Unertl, Au(110) (1 × 2)-to-(1 × 1) phase transition: a physical realization of the two-dimensional Ising model, *Phys. Rev. Lett.* 54 (1985) 2684–2687.
- [60] P.I. Kuzmin, S.A. Akimov, Y.A. Chizmadzhev, J. Zimmerberg, F.S. Cohen, Line tension and interaction energies of membrane rafts calculated from lipid splay and tilt, *Biophys. J.* 88 (2005) 1120–1133.
- [61] S.A. Akimov, P.I. Kuzmin, J. Zimmerberg, F.S. Cohen, Y.A. Chizmadzhev, An elastic theory for line tension at a boundary separating two lipid monolayer regions of different thickness, *J. Electroanal. Chem.* 564 (2004) 13–18.
- [62] W.C. Tsai, G.W. Feigenson, Lowering line tension with high cholesterol content induces a transition from macroscopic to nanoscopic phase domains in model biomembranes, *Biochim. Biophys. Acta Biomembr.* 2019 (1861) 478–485.
- [63] E. Rufeil Fiori, R. Downing, G. Volpe Bossa, S. May, Influence of spontaneous curvature on the line tension of phase-coexisting domains in a lipid monolayer: a Landau-Ginzburg model, *J. Chem. Phys.* 152 (2020).
- [64] R.G. Oliveira, B. Maggio, Surface behavior, microheterogeneity and adsorption equilibrium of myelin at the air-water interface, *Chem. Phys. Lipids* 122 (2003) 171–176.

- [65] K. Larsson, in: F.D. Gunstone, J.L. Harwood, F.B. Padley (Eds.), *The Lipid Handbook*, Chapman and Hall, London, 1994, pp. 419–422.
- [66] T. Wang, T. Muzic, A.D. Jackson, T. Heimburg, The free energy of biomembrane and nerve excitation and the role of anesthetics, *Biochim. Biophys. Acta Biomembr.* 2018 (1860) 2145–2153.
- [67] J. Trager, K. Widder, A. Kerth, G. Harauz, D. Hinderberger, Effect of cholesterol and myelin basic protein (MBP) content on lipid monolayers mimicking the cytoplasmic membrane of myelin, *Cells* 9 (2020).